AN ASSESSMENT TOOL ON ACTIVE/PASSIVE CONTROL METHODOLOGIES FOR WHIRL FLUTTER STABILITY IN TILTROTOR AIRCRAFTS

Taeseong Kim[1] and SangJoon Shin[2]

[1] School of Mechanical and Aerospace Engineering
Seoul National University
San 56-1, Shillim-Dong, Gwanak-Gu, Seoul 151-742, Korea
e-mail: kimts77@snu..ac.kr

[2] School of Mechanical and Aerospace Engineering
Seoul National University
San 56-1, Shillim-Dong, Gwanak-Gu, Seoul 151-742, Korea
e-mail: ssjoon@snu..ac.kr

Key words: Unsteady aerodynamics, Whirl flutter, Stability boundary, Tiltrotor aircraft

Abstract: The whirl flutter phenomenon is induced by excessive inplane hub forces, and imposes a serious limit on the forward speed in tiltrotor aircraft. Therefore, it is necessary to investigate the whirl flutter instability to increase the maximum aircraft speed. In this paper, based on Greenberg model, quasi-steady and unsteady aerodynamic forces are formulated to examine the whirl flutter stability for a three-bladed rotor without flexible wing modes. Numerical results are obtained in both time and frequency domain. Among them, generalized eigenvalue is utilized to estimate whirl flutter stability in frequency domain, and Runge Kutta method is used to analyze in time domain. The effects of varying the pylon spring stiffness and the swashplate geometric control coupling upon the flutter boundary are also investigated.

1 INTRODUCTION

Since the phenomenon of whirl flutter was discovered in the early 1960s for the first time, quite a few investigations have been conducted because the whirl flutter instability, which is induced by excessive inplane hub forces, imposes a limit on the forward speed in the tiltrotor aircrafts. Investigation of the whirl flutter instability is therefore necessary to increase the maximum aircraft speed. However the problem has not been clearly solved yet. Whirl flutter involves two modes of the tiltrotor aircrafts, which are a rotor and a pylon mode. The rotor mode is the backward whirl mode which occurs at low frequencies while the pylon mode is the forward whirl mode whose flutter frequencies are near the natural frequencies of the aircraft system. Flutter frequencies of the pylon mode are higher than those associated with flutter in the rotor mode. There exists a significant difference between the two flutter mechanisms. In the pylon mode the precession is in the same direction as the rotor blade rotation. On the other hand, the precession of the rotor mode is in the opposite direction. It has been found that the whirl flutter instability occurs more frequently in the rotor mode because of the low frequencies.[1,2]

The whirl flutter does not occur at low inflow condition. However, it becomes a serious issue at high inflow condition, such as an airplane-mode cruise flight in tiltrotor aircrafts. The aerodynamic forces and moments of the rotor blade are generated according to the local angle of attack change on each blade element. It causes precession of the whole rotor blade, which in

turn provides the mechanism for instability. The mechanism of the whirl flutter is illustrated in Figure 1 for a two-bladed rotor. Under the high inflow condition, the angle of attack at a representative 75% spanwise location, $\Delta\alpha$, has a negative value at Blade No. 2 instantaneously. The lift component, ΔL, appears perpendicular to the control plane. This lift component is divided into a thrust, ΔT, and a H-force component, ΔH. Precession of the rotor blade is created by the H-force components both in Blade Nos. 1 and 2, because these forces act in the same direction. At the same time, high transient flapping is caused by the thrust component, ΔT, because these forces act in the opposite direction. Due to these aerodynamic forces and moments, whirl flutter instability occurs in tiltrotor aircrafts.[1]

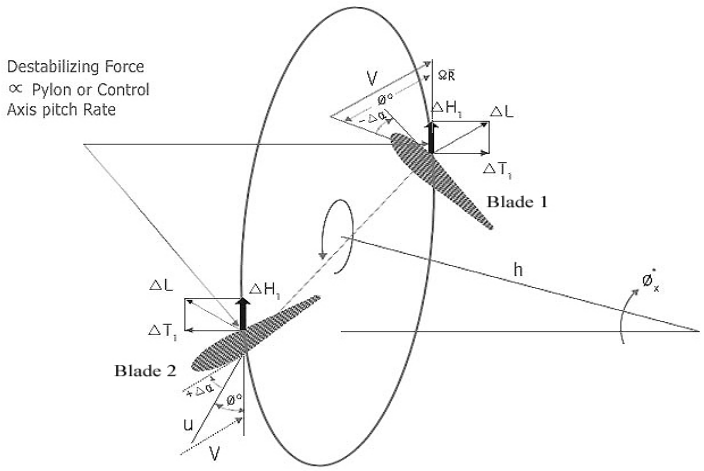

Figure 1: Mechanism of the whirl flutter

To improve the stability boundary in tiltrotor aircrafts, Hall examined some passive control methodologies analytically, such as pitch-flap coupling and the pylon stiffness parameters.[1] Stability of the proprotor pylon system was affected to a certain degree by these control methods. Active control with an optimal algorithm was investigated analytically to improve tiltrotor gust response by Johnson.[3] A feedback controller based on a linear system was designed to minimize a quadratic performance index. The actuation strategies were applied on the active flaperon in that study, which were effective in improving the gust response. In Ref. 4, Higher Harmonic Control (HHC) was experimentally employed at both the rotor swashplate and the wing flaperon to reduce vibrations induced in airplane mode. The effectiveness of the swashplate and the wing flaperon acting either in single or combination mode was demonstrated in reducing 1/rev and 3/rev wing vibration. In 1990's Generalized Predictive Control (GPC), which is a digital time domain multi-input multi-output predictive control method, was experimentally investigated to evaluate the effectiveness of an adaptive control algorithm. Active control was introduced into fixed-system swashplate using three high-frequency servo-controlled hydraulic actuators mounted aft of the swashplate inside the pylon fairing.[5,6] The GPC algorithm was highly effective in increasing the stability in the critical wing mode of the model tested. However it turned out to be a very complex algorithm, therefore it was not attractive. More recently, another active control algorithm employed via actuation of the wing flaperon and the rotor swashplate was examined for whirl flutter stability and robustness augmentation.[5] Full state feedback, which was composed of Linear Quadratic Regulator (LQR) optimal control and wing state feedback control, was used in that investigation.

From the survey described above, it is observed that the previous analytical investigations have not considered two important phenomena. First, unsteady aerodynamic formulation needs to be included in order to represent more realistic aerodynamic environment generated in tiltrotor aircrafts. Second, interference between the rotor blades and the wing has to be taken into account because it is a principal source of the rotor induced airframe vibration. By including these two effects, it is possible to establish a more complete analytical model, which is capable of a quite accurate prediction. An immediate goal of the present paper is to develop an analytical framework with these factors included and validate it against other analytical or experimental results.

In this paper, a gimballed stiff-inplane three-bladed rotor system is used to investigate its whirl flutter stability and the related stability boundary. An assessment tool on passive control methodologies for whirl flutter stability in tiltrotor aircrafts is also developed. Numerical results are obtained using the present tool in time and frequency domain. Generalized eigenvalue solution is used to estimate whirl flutter instability in frequency domain, while Runge Kutta method is used to analyze in time domain.

2 DESCRIPTION OF THE MODEL

2.1 Structural Dynamic Model

The structural model, which is shown in Fig. 2, is developed based on Ref. 7. The present model consists of four degrees of freedom, which are two rotor blade flapping angles (β_{1C} and β_{1S}), and pitch and yaw angles (α_y and α_x) of the pylon. Positive direction of the flapping motion is defined for forward displacement of the blade tip from the disk plane. Positive direction of the pitch angle for the pylon and yaw are defined for upward and left rotation of the hub, respectively. A flapping motion of the rotor is assumed to be composed of the totally rigid three blades.

Using the forces and moments equilibrium, equations of the structural inertia, damping, and stiffness are obtained as follows.

$$I_b\left(\ddot{\beta}_m + \nu_\beta{}^2\beta_m - \left(\ddot{\alpha}_y - 2\Omega\dot{\alpha}_x\right)\cos\psi_m + \left(\ddot{\alpha}_x + 2\Omega\dot{\alpha}_y\right)\sin\psi_m\right) = M_{F_m} \qquad (1)$$

$$I_x\ddot{\alpha}_x + C_x\dot{\alpha}_x + K_x\alpha_x = M_x - hY \qquad (2)$$

$$I_y\ddot{\alpha}_y + C_y\dot{\alpha}_y + K_y\alpha_y = M_y + hH \qquad (3)$$

Eqs. (1), (2), and (3) are respectively flap, yaw, and pitch moment equilibrium equations. Employing the Fourier coordinate transformation, it is possible to convert these into the equations in the nonrotating frame. These equations are dimensionless with ρ, Ω, R, I_b, γ, σ, and $I_b(N/2)$. The equations of motion for four degrees of freedom can be represented as a matrix form as in Eq. (4).

$$\underbrace{\begin{bmatrix} 1 & 0 & -1 & 0 \\ 0 & 1 & 0 & 1 \\ 0 & 0 & I_y^* & 0 \\ 0 & 0 & 0 & I_x^* \end{bmatrix}\begin{pmatrix} \ddot{\beta}_{1C} \\ \ddot{\beta}_{1S} \\ \ddot{\alpha}_y \\ \ddot{\alpha}_x \end{pmatrix} + \begin{bmatrix} 0 & 2 & 0 & 2 \\ -2 & 0 & 2 & 0 \\ 0 & 0 & C_y^* & 0 \\ 0 & 0 & 0 & C_x^* \end{bmatrix}\begin{pmatrix} \dot{\beta}_{1C} \\ \dot{\beta}_{1S} \\ \dot{\alpha}_y \\ \dot{\alpha}_x \end{pmatrix} + \begin{bmatrix} \nu_\beta^2 - 1 & 0 & 0 & 0 \\ 0 & \nu_\beta^2 - 1 & 0 & 0 \\ 0 & 0 & K_y^* & 0 \\ 0 & 0 & 0 & K_x^* \end{bmatrix}\begin{pmatrix} \beta_{1C} \\ \beta_{1S} \\ \alpha_y \\ \alpha_x \end{pmatrix}}_{\textit{Structural Dynamic Model}}$$

$$= \underbrace{\gamma \begin{pmatrix} M_{F_{1C}} / ac \\ M_{F_{1S}} / ac \\ 2C_{M_y} / \sigma a + h(2C_H / \sigma a) \\ 2C_{M_x} / \sigma a - h(2C_y / \sigma a) \end{pmatrix}}_{\textit{Aerodynamic Model}} \tag{4}$$

The structural dynamic and aerodynamic parts are organized in the right hand side (RHS) and left hand side (LHS) in Eq. (4), respectively.

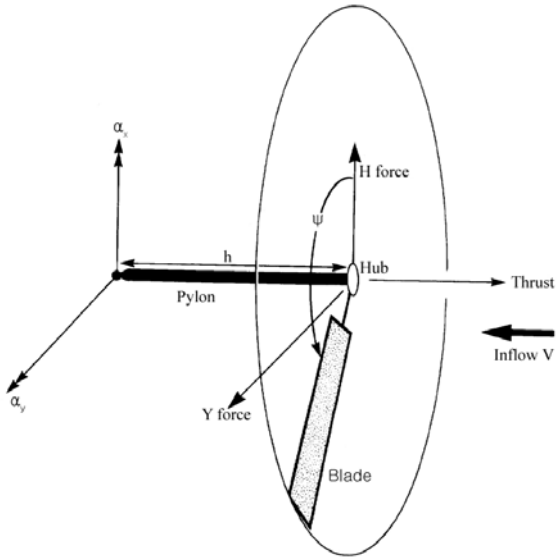

Figure 2: Totally rigid bladed rotor system

2.2 Aerodynamic Model

The rotor is assumed to be operating in a purely axial flow in the equilibrium. When evaluating the blade forces and moments, each velocity component has a trim and a perturbation component. However, only perturbation component is considered to evaluate whirl flutter stability in this paper. Trim state is assumed to be established already and the perturbation from it is considered for flutter analysis.

The rotor aerodynamic forces and moments are presented in the RHS of Eq. (4). Three different kinds of aerodynamic models, which are two quasi-steady and an unsteady aerodynamic model, are now developed to predict whirl flutter stability both in time and frequency domain. The first aerodynamic model is widely used and is quoted as a normal quasi-steady aerodynamics in this paper. This aerodynamic model is developed based on Ref. 7, and, is described in Eq. (5). The second quasi-steady aerodynamic model is presented in Eq. (6). It is equivalent to replacing $C(k)$ by 1 in Greenberg's aerodynamic model.[8,9] In Eq. (6), noncirculatory part is ignored because the most terms are eliminated by the coordinate transformation and the effects of the remaining terms are very small. This model is quoted as Greenberg's quasi-

steady aerodynamics in this paper. For a full unsteady aerodynamic representation, Greenberg 's two-dimensional unsteady aerodynamic model,[9] which is extended to account for time-varying incoming airspeed, is used.[10] Its expression is presented in Eq. (7).

$$L = 2\pi\rho U(t)^2 b\alpha(t) \tag{5}$$

$$L = 2\pi\rho U(t)b[(\dot{h}(t) + U(t)\theta(t)) + b(\frac{1}{2} - a_h)\dot{\theta}(t)_{ref}] \tag{6}$$

$$L = \underbrace{2\pi\rho U(t)bC(k)[(\dot{h}(t) + U(t)\theta(t)) + b(\frac{1}{2} - a_h)\dot{\theta}(t)_{ref}]}_{Circulatory\ part(L_C)} + \underbrace{\pi\rho b^2[(\dot{h}(t) + U(t)\theta(t))\dot{} - ba_h\ddot{\theta}(t)_{ref}]}_{Noncirculatory\ part(L_{NC})} \tag{7}$$

The aerodynamic environment of the rotor blade typical section is shown in Fig. 3. All the velocities and forces are estimated with respect to the hub plane, which is used as a reference frame. The aerodynamic forces on the blade typical section are lift (L), and drag (D).

According to Fig. 3, total forces in x and z direction can be obtained as follows.

$$\frac{\bar{F}_z}{ac} = \frac{\bar{L}}{ac}\cos\phi - \frac{\bar{D}}{ac}\sin\phi \tag{8}$$

$$\frac{\bar{F}_x}{ac} = \frac{\bar{L}}{ac}\sin\phi + \frac{\bar{D}}{ac}\cos\phi \tag{9}$$

where, $\sin\phi = \frac{u_p(\psi)}{U(\psi)}$, and $\cos\phi = \frac{u_T(\psi)}{U(\psi)}$. $\bar{L}$ and $\bar{D}$ are the modified factors of L and D, which are divided by $\rho\Omega^2R^3$. These factors will be dimensionless, therefore Eqs. (8) and (9) describe dimensionless quantities.

Drag forces can be neglected because they are relatively small compared to the lift forces. Then Eqs. (8) and (9) can be simplified as follows.

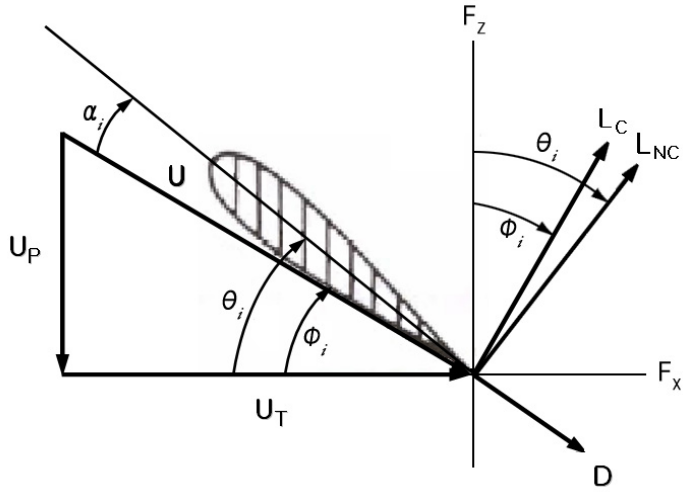

Figure 3: Resultant velocity and inflow velocity on the typical blade section

$$\frac{\bar{F}_z}{ac} = \frac{\bar{L}}{ac}\frac{u_T(\psi)}{U(\psi)} \tag{10}$$

$$\frac{\bar{F}_x}{ac} = \frac{\bar{L}}{ac}\frac{u_P(\psi)}{U(\psi)} \tag{11}$$

$$\frac{\bar{F}_r}{ac} = \bar{U}\bar{u}_R\frac{C_d}{2a} - \beta\frac{\bar{F}_z}{ac} \simeq -\beta\frac{\bar{F}_z}{ac} \tag{12}$$

Above equations can be used for the two quasi-steady aerodynamic models. However, it is impossible to obtain the forces and moments by using the above equations in the full unsteady aerodynamic model, because there are certainly two parts in the expression, which are noncirculatory and circulatory part. These parts are clearly presented in Eq. (7). The lift deficiency function, $C(k)$, can be represented only in frequency domain as in Eq. (7). Therefore Jones' approximation[11,12] is utilized as follows.

$$C(k) = \left[\frac{0.5\bar{s}^2 + 0.2808\bar{s} + 0.01365}{\bar{s}^2 + 0.3455\bar{s} + 0.01365}\right] \tag{13}$$

where $\bar{s} = s\dfrac{\bar{b}R}{U_0}$.

By substituting Eq. (13) into Eq. (7), a state space equation is obtained as follows.

$$\begin{aligned}\begin{Bmatrix}\dot{X}_1\\ \dot{X}_2\end{Bmatrix} &= \begin{bmatrix}a_{11} & a_{12}\\ 1 & 0\end{bmatrix}\begin{Bmatrix}X_1\\ X_2\end{Bmatrix} + \begin{Bmatrix}1\\ 0\end{Bmatrix}Q(t)\\ y &= \begin{bmatrix}C & D\end{bmatrix}\begin{Bmatrix}X_1\\ X_2\end{Bmatrix} + 0.5Q(t)\end{aligned} \tag{14}$$

where, $Q(t) = \left[(\dot{h}(t) + U(t)\alpha(t)) + b(\frac{1}{2} - a_h)\dot{\theta}(t)_{ref}\right]$, $a_{11} = -0.3455\left(\dfrac{U_0}{\bar{b}R}\right)$, $a_{12} = -0.0137\left(\dfrac{U_0}{\bar{b}R}\right)^2$, $C = 0.1081\left(\dfrac{U_0}{\bar{b}R}\right)$, and $D = 0.0068\left(\dfrac{U_0}{\bar{b}R}\right)^2$.

From Eq. (14), new state space equations for the augmented state variables and circulatory part of the lift can be formulated as follows.

$$\begin{aligned}\begin{Bmatrix}\dot{\bar{X}}_1\\ \dot{\bar{X}}_2\end{Bmatrix} &= \begin{bmatrix}a_{11} & a_{12}\\ 1 & 0\end{bmatrix}\begin{Bmatrix}\bar{X}_1\\ \bar{X}_2\end{Bmatrix} + \begin{Bmatrix}1\\ 0\end{Bmatrix}Q(\psi)\\ \bar{L}_c &= 2\pi bU(\psi)\left\{C\bar{X}_1 + D\bar{X}_2 + 0.5Q(\psi)\right\}\end{aligned} \tag{15}$$

where, $X_1 = R\bar{X}_1$, $X_2 = \dfrac{R}{\Omega}\bar{X}_2$, and $\dfrac{\partial}{\partial t} = \Omega\dfrac{\partial}{\partial\psi}$.

Eq. (15) can be used to replace the circulatory part in Eq. (7). Noncirculatory part is not considered anymore. Therefore an updated lift expression is obtained as follows, which can be computed only in time domain.

$$\bar{L} = \underbrace{2\pi \bar{b} U(\psi)\left\{C\bar{X}_1 + D\bar{X}_2 + 0.5Q(\psi)\right\}}_{\bar{L}_C} \tag{16}$$

In Eq. (16), the augmented state variables, $\bar{X}_1$ and $\bar{X}_2$, are governed by a system of ordinary differential equations, and associated with a downwash velocity at the three quarter chord location.[13] These augmented states are driven by the time history of $Q(\psi)$ at each spanwise location. However, the augmented state variables of the typical section at ¾ span location are utilized as an averaged value in this paper. A Fourier coordinate transformation may be applied to express, $Q(\psi)$, $\bar{X}_1$, and $\bar{X}_2$ in the nonrotating coordinate system:

$$\begin{aligned} Q(\psi) &= \bar{Q}_0 + \sum_{n=1}^{NH} \bar{Q}_{1cn}\cos n\psi + \bar{Q}_{1sn}\sin n\psi \\ \bar{X}_1 &= \bar{X}_{1_0} + \sum_{n=1}^{NH} \bar{X}_{1cn}\cos n\psi + \bar{X}_{1sn}\sin n\psi \\ \bar{X}_2 &= \bar{X}_{2_0} + \sum_{n=1}^{NH} \bar{X}_{2cn}\cos n\psi + \bar{X}_{2sn}\sin n\psi \end{aligned} \tag{17}$$

By substituting Eq. (17) into Eq. (16), it is possible to obtain the lift in the full unsteady aerodynamic model for an analysis in time domain. According to Fig. 3, total forces in each direction are obtained as in Eqs. (10) and (11).

Figure 4 shows the inplane forces, which are *H* and *Y* forces on each blade.

From Fig. 4, the inplane forces can be expressed as follows.

$$\begin{aligned} H \text{ force } &= F_x \sin\psi_m + F_r \cos\psi_m \\ Y \text{ force } &= -F_x \cos\psi_m + F_r \sin\psi_m \end{aligned} \tag{18}$$

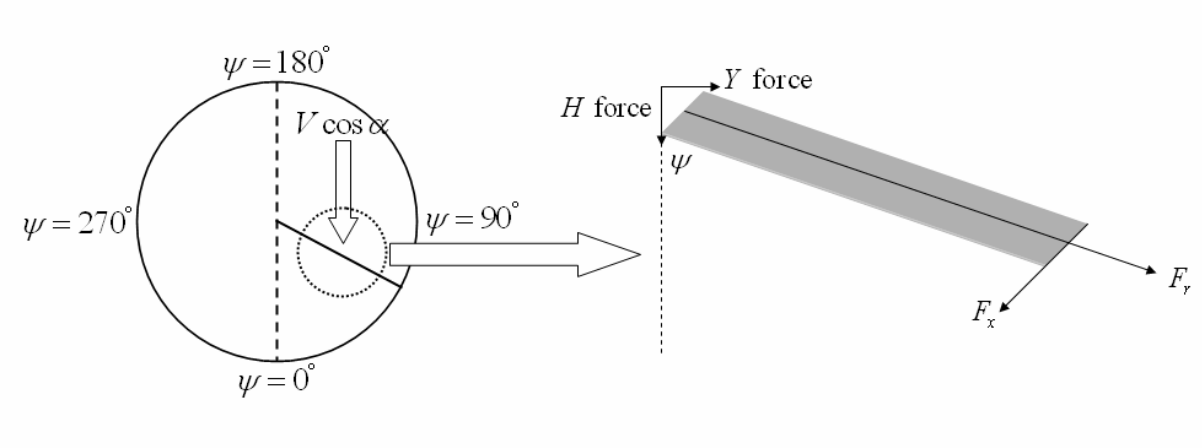

Figure 4: H and Y forces on the blade

The net rotor aerodynamic forces and moments are obtained by integrating the section forces and moments over the span of the blade and summing over all the three blades.

$$
\begin{aligned}
\frac{C_T}{\sigma a} &= \frac{1}{N}\sum_m \int_0^1 \frac{\bar{F}_z}{ac}\,dr \\
\frac{2C_H}{\sigma a} &= \frac{2}{N}\sum_m (\cos\psi_m \int_0^1 \frac{\bar{F}_r}{ac}\,dr + \sin\psi_m \int_0^1 \frac{\bar{F}_x}{ac}\,dr) \\
\frac{2C_Y}{\sigma a} &= \frac{2}{N}\sum_m (\sin\psi_m \int_0^1 \frac{\bar{F}_r}{ac}\,dr - \cos\psi_m \int_0^1 \frac{\bar{F}_x}{ac}\,dr) \\
\frac{\bar{M}_F}{ac} &= \int_0^1 r\frac{\bar{F}_z}{ac}\,dr
\end{aligned}
\tag{19}
$$

The pitch and yaw moments of the hub due to the rotor are now formulated. The source of the hub moment is the bending moment at the blade rotor due to the flapping, $M_m = I_b(\nu_\beta^2 - 1)\beta^m$. Therefore, the rotor lateral and longitudinal moment coefficients are formulated as follows.

$$
\frac{2C_{My}}{\sigma a} = -\frac{\nu_\beta{}^2 - 1}{\gamma}\beta_{1c} \tag{20}
$$

$$
\frac{2C_{Mx}}{\sigma a} = \frac{\nu_\beta{}^2 - 1}{\gamma}\beta_{1s} \tag{21}
$$

2.3 Governing Equations

After obtaining the rotor forces and moments as in Eqs. (19), (20), and (21), these quantities are substituted into the RHS in Eq. (4). The governing equation is obtained for the four degrees of freedom. In this paper, three different kinds of aerodynamic models are used, thus the three different governing equations are obtained as follows.

I. Two Quasi-steady Aerodynamic Models

Putting the forces and moments of the rotor, which are expressed in Eqs. (5) and (6), into the RHS of Eq. (4) gives the following expression.

$$
RHS = C_a\dot{y} + K_a y \tag{22}
$$

where $y^T = \begin{pmatrix} \beta_{1C} & \beta_{1S} & \alpha_y & \alpha_x \end{pmatrix}$ and the subscript *a* means an aerodynamic part.

The governing equation can be obtained as follows.

$$
M_s\ddot{y} + C_s\dot{y} + K_s y = C_a\dot{y} + K_a y \tag{23}
$$

where the subscript *s* means a structural part and all elements of matrices are dimensionless quantities.

For simplicity, Eq. (23) can be rearranged as

$$
\begin{aligned}
M_s\ddot{y} &= -(C_s - C_a)\dot{y} - (K_s - K_a)y \\
\therefore \ddot{y} &= -M_s{}^{-1}(C_s - C_a)\dot{y} - M_s{}^{-1}(K_s - K_a)y = -(M^{-1}\bar{C})\dot{y} - (M^{-1}\bar{K})y = -A\dot{y} - By
\end{aligned}
\tag{24}
$$

where, $\bar{C} = (C_s - C_a)$, $\bar{K} = (K_s - K_a)$, $A = (M^{-1}\bar{C})$, and $B = (M^{-1}\bar{K})$.

Converting Eq. (24) into a state space form gives

$$\dot{Y} = \underbrace{\begin{bmatrix} 0 & I \\ -B & -A \end{bmatrix}}_{8\times 8} \underbrace{\begin{Bmatrix} y \\ \dot{y} \end{Bmatrix}}_{8\times 1} \tag{25}$$

where $Y^T \equiv \{ y \quad \dot{y} \}$.

II. Full Unsteady Aerodynamic Models

The method for deriving the governing equation is similar to that for quasi-steady aerodynamic models. However, the present governing equation needs to include an ordinary differential equation for the augmented state variables, in addition to Eq. (4).

Substituting the rotor forces and moment, which are obtained at the hub frame, into the aerodynamic part in Eq. (4), a state space equation is obtained as follows.

$$\dot{Y} = \underbrace{\begin{bmatrix} 0 & I \\ -B & -A \end{bmatrix}}_{8\times 8} \underbrace{\begin{Bmatrix} y \\ \dot{y} \end{Bmatrix}}_{8\times 1} + \underbrace{\begin{Bmatrix} 0 \\ C \end{Bmatrix}}_{8\times 4} \underbrace{X}_{4\times 1} \tag{26}$$

where $X^T = \left(\bar{X}_{1C} \quad \bar{X}_{1S} \quad \bar{X}_{2C} \quad \bar{X}_{2S} \right)$.

Eqs. (26) and (15) can be simplified to be

$$\begin{aligned} \dot{Y} &= \underbrace{T^*}_{8\times 8} \underbrace{Y}_{8\times 1} + \underbrace{S^*}_{8\times 4} \underbrace{X}_{4\times 1} \\ \dot{X} &= \underbrace{E}_{4\times 4} \underbrace{X}_{4\times 1} + \underbrace{D}_{4\times 8} \underbrace{Y}_{8\times 1} \end{aligned} \tag{27}$$

where $T^* = \underbrace{\begin{bmatrix} 0 & I \\ -B & -A \end{bmatrix}}_{8\times 8}$, $S^* = \underbrace{\begin{Bmatrix} 0 \\ C \end{Bmatrix}}_{8\times 4}$, $E = \begin{bmatrix} a_{11} & a_{12} \\ 1 & 0 \end{bmatrix}$, $D = \begin{Bmatrix} 1 \\ 0 \end{Bmatrix}$, $A = (\bar{M}^{-1}\bar{C})$, $B = (\bar{M}^{-1}\bar{K})$,

$C = (\bar{M}^{-1} Z_a)$, $\bar{M} = (M_s - M_a)$, $\bar{C} = (C_s - C_a)$, and $\bar{K} = (K_s - K_a)$

Combining each quantity in Eq. (27), the following governing equation, which enables analysis both in time and frequency domain, is obtained in a state space form.

$$\begin{bmatrix} \dot{Y} \\ \dot{X} \end{bmatrix} = \underbrace{\begin{bmatrix} \underbrace{T^*}_{8\times 8} & \underbrace{S^*}_{8\times 4} \\ \underbrace{D}_{4\times 8} & \underbrace{E}_{4\times 4} \end{bmatrix}}_{12\times 12} \underbrace{\begin{bmatrix} Y \\ X \end{bmatrix}}_{12\times 1} \tag{28}$$

where all elements of matrices are dimensionless quantities.

3 NUMERICAL RESULTS

Numerical investigation is conducted in order to obtain whirl flutter stability boundary in time and frequency domain based on each aerodynamic model. Two passive control algorithms, which are variation of the pylon stiffness and the pitch-flap coupling, are also attempted to evaluate whirl flutter stability boundary in both domain analyses.

It is assumed that the trim state is already established, therefore only perturbation effects are considered to obtain the results regarding whirl flutter stability analysis in this paper. Any other control pitch input and gust effects are not included. The perturbation velocities are defined as follows.

$$\delta U = \frac{u_{T_0}}{U_0}\delta u_T + \frac{u_{p_0}}{U_0}\delta u_p \tag{29}$$

$$\delta u_p = r(\dot{\beta} - \dot{\alpha}_y \cos\psi_m + \dot{\alpha}_x \sin\psi_m) = r\delta u_{p_B} \tag{30}$$

$$\delta u_T = -h(\dot{\alpha}_y \sin\psi_m + \dot{\alpha}_x \cos\psi_m) + (V+v)(\alpha_y \sin\psi_m + \alpha_x \cos\psi_m) \tag{31}$$

In order to investigate whirl flutter stability, aircraft flight velocity is increased and its stability is evaluated while keeping the same structural parameters, such as $h = 0.261$, $\gamma = 3.83$, $\nu_\beta = 1.02$, $\xi = 0.04$, $\Omega = 458RPM$, and $b = 0.047$, which are dimensionless quantities. All the structural and aerodynamic quantities in this paper are dimensionless values. Among them, structural parameters are based on those in Johnson's work.[7]

I. Normal Quasi-steady Aerodynamic Models

This section presents the results of the normal quasi-steady aerodynamic model in which the lift is expressed as in Eq. (5). Figure 5 illustrates the results of the stability analysis in time and frequency domain while increasing aircraft speed from 276 to 306 ft/sec. Figure 5(a) shows the results of time domain analysis while increasing aircraft speed. It is shown that the system is stable at V =276 ft/sec. However, the current system becomes unstable when increasing the aircraft speed to 306 ft/sec. Figure 5(b) explains the results of the frequency domain analysis at the same aircraft speed range. In this aerodynamic model, it is observed that stability boundary is approximately 296 ft/sec, which is considered to be a realistic whirl flutter boundary in the present tiltrotor aircraft.

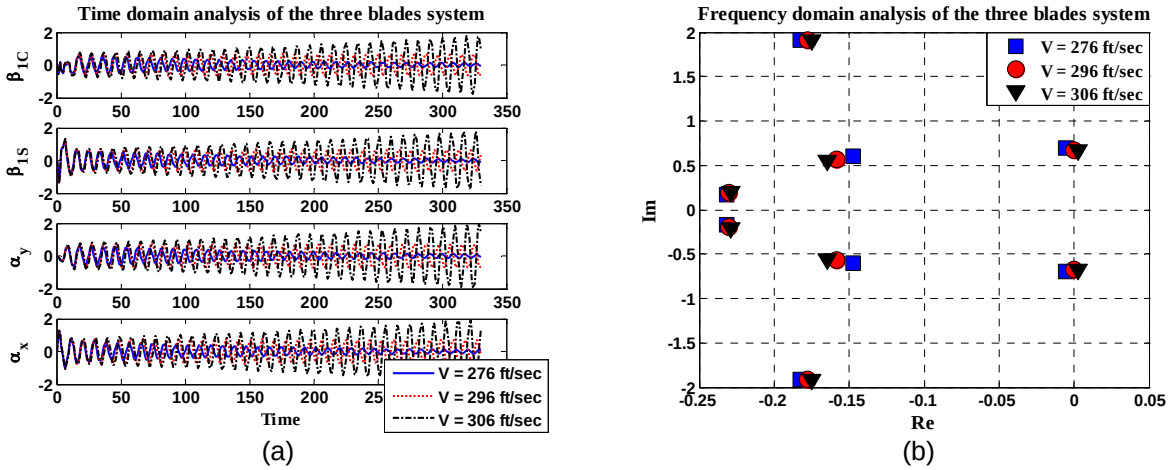

Figure 5: Time and frequency domain analysis using the normal quasi-steady aerodynamics

Passive control algorithms are applied such as variation of the pylon stiffness and the pitch-flap coupling (δ_3). Figure 6 shows the results of the pylon stiffness variation in time domain. The nominal aircraft speed is 296 ft/sec, which is obtained as the flutter boundary by time domain analysis as above. The flutter velocity can be improved by increasing the pylon stiffness. Figure 6 indicates that the flutter boundary is almost linearly increased by the increment of the pylon stiffness until 20% relative to the nominal value. Figure 7 shows whirl flutter stability variation of the pitch-flap coupling from -15 to 30° in the rotor system. It is observed that there is an effective range of the pitch-flap coupling which can improve flutter stability boundary. In this aerodynamic model, an optimum pitch-flap coupling is approximately 10°. When it is lower or upper than 10°, the system stability may be decreased.

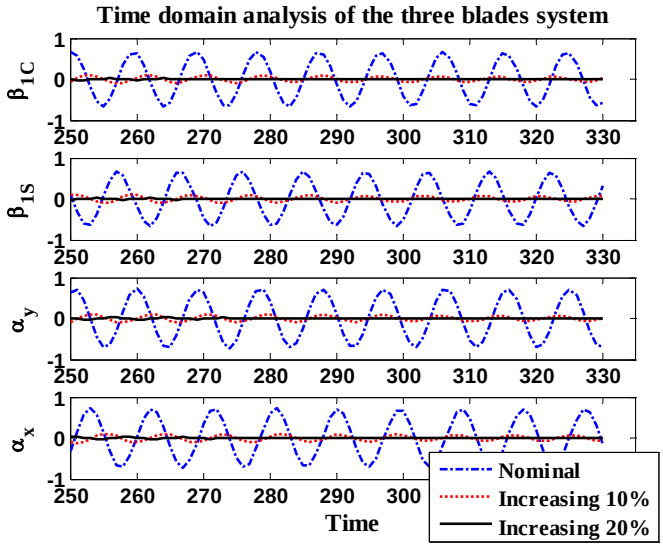

Figure 6: Results with respect to the pylon stiffness at V=296(ft/sec)

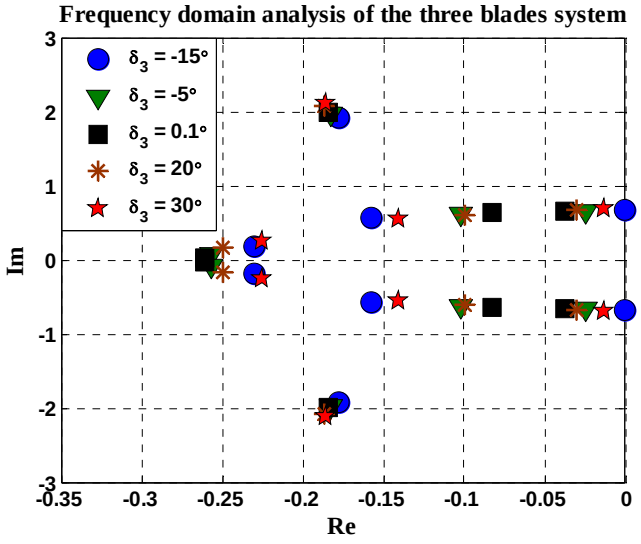

Figure 7: Results with respect to δ_3 at V=296(ft/sec)

II. Greenberg's Quasi-steady Aerodynamic Models

This aerodynamic model has a similar formulation with that in the normal quasi-steady aerodynamics. However, the lift formulation has a few different terms. According to Eq. (6), the first-order time derivative terms, which are $\dot{h}$ and $\dot{\theta}_{ref}$, are newly included in Greenberg's quasi-steady aerodynamics. Here, $\dot{h}$ is velocity of the flapping motion, which is $-\delta u_P$, while $\dot{\theta}_{ref}$ is angular velocity of the pitch motion with respect to the inertial frame.

The perturbation terms are only utilized in this model as in the normal quasi-steady aerodynamics. Therefore, the perturbation term of θ_{ref} is organized as follow.

$$\delta\theta_{ref} = -K_p\beta + \alpha_y \cos\psi + \alpha_x \sin\psi \tag{32}$$

Substituting Eqs. (29)-(32) into (7), the lift forces can be obtained, and then all the forces and moments acting at hub are obtained in the hub reference frame.

Figure 8 shows the results of whirl flutter stability in time and frequency domain using Greenberg's quasi-steady aerodynamics. According to Fig. 8(a), which is a time domain analysis result, the flutter boundary is *V*=294 ft/sec. It is possible to check the flutter stability also by frequency domain analysis, as in Fig. 8(b). When the aircraft speed is 294 ft/sec, the system poles are located on imaginary axis. There is a slight discrepancy between the normal and Greenberg's aerodynamic model. The present Greenberg's quasi-steady aerodynamics gives a little more conservative flutter velocity result than the normal quasi-steady one does.

Under Greenberg's aerodynamic model, one of the passive control algorithms, which is varying the pitch-flap coupling, is implemented to improve stability characteristics. Figure 9 illustrates the result of the δ_3 effects from -15 to 20° in the frequency domain. According to Fig. 9, an optimum δ_3 coupling is obtained to be approximately 0°.

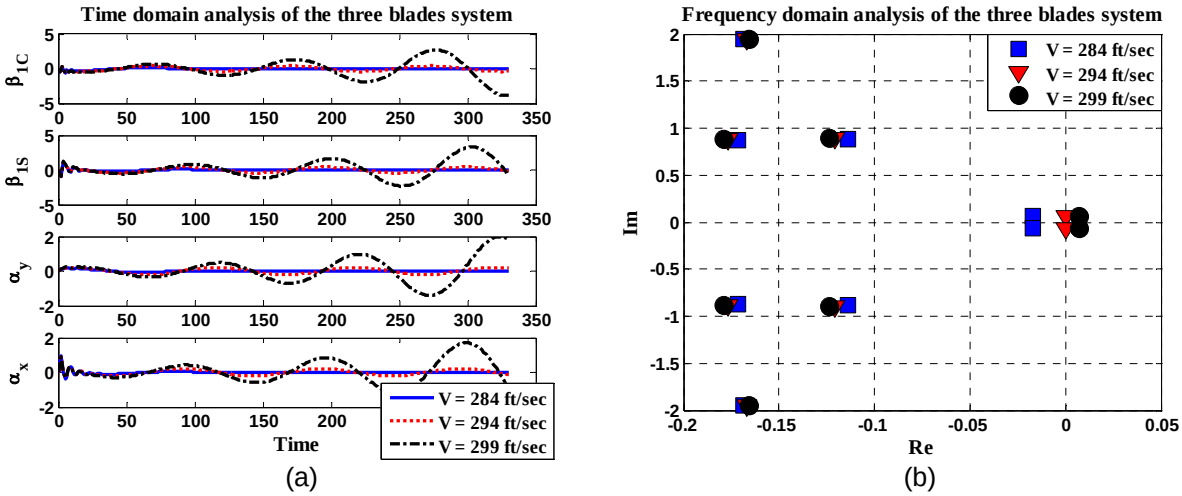

Figure 8: Time and frequency domain analysis using Greenberg's quasi-steady aerodynamics

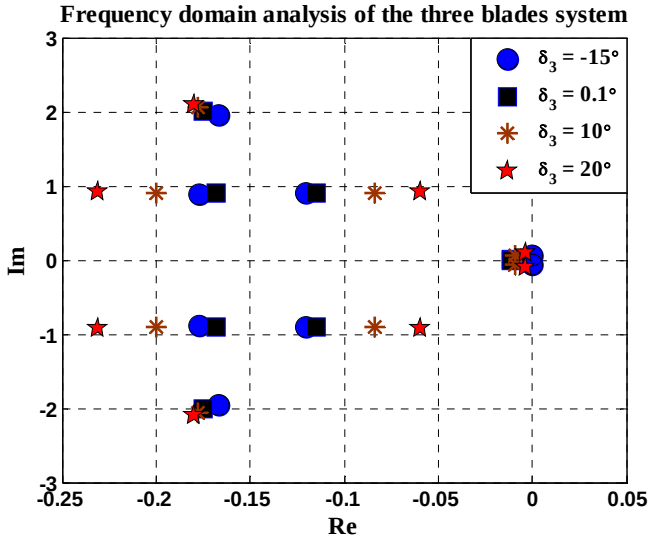

Figure 9: Results with respect to δ_3 at V=294(ft/sec)

III. Full Unsteady Aerodynamic Models

As mentioned previously, quasi-steady aerodynamic model is not capable of describing a realistic aerodynamic environment occurred in tiltrotor aircraft. In this section, numerical investigation is presented using Greenberg's two-dimensional unsteady aerodynamic model. The difference between Greenberg's quasi-steady and the full unsteady aerodynamics is the inclusion of the lift deficiency function in the latter model.

Figure 10 illustrates the time and frequency results of the two-dimensional airfoil while increasing aircraft speed from 349 to 362 ft/sec. According to Fig. 10(a) and (b), the stability boundary becomes 359 ft/sec based on the full unsteady aerodynamics. These results are much less conservative than those based on the quasi-steady aerodynamic models are.

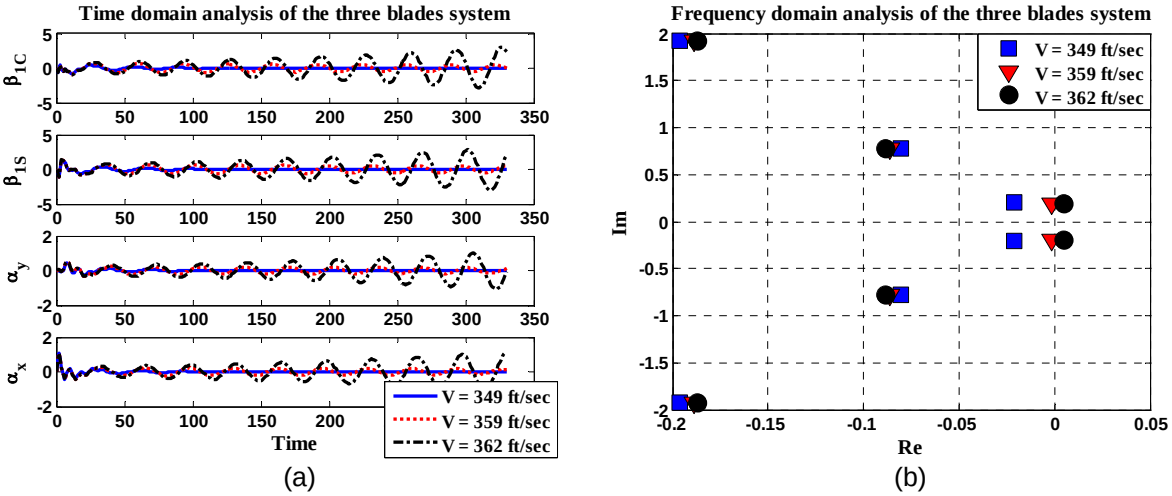

Figure 10: Time and frequency domain analysis using the full unsteady aerodynamics

Figure 11 shows comparison of the whirl flutter stability in time and frequency domain among the three aerodynamic models. This comparison clearly shows that the whirl flutter

stability is overestimated by the full unsteady aerodynamic model. Between the normal and Greenberg's quasi-steady aerodynamic model, stability boundary is decreased by approximately 1% by the latter. Moreover, compared with Greenberg's quasi-steady aerodynamic model, flutter boundary is predicted to increase by approximately 20% by the full unsteady model.

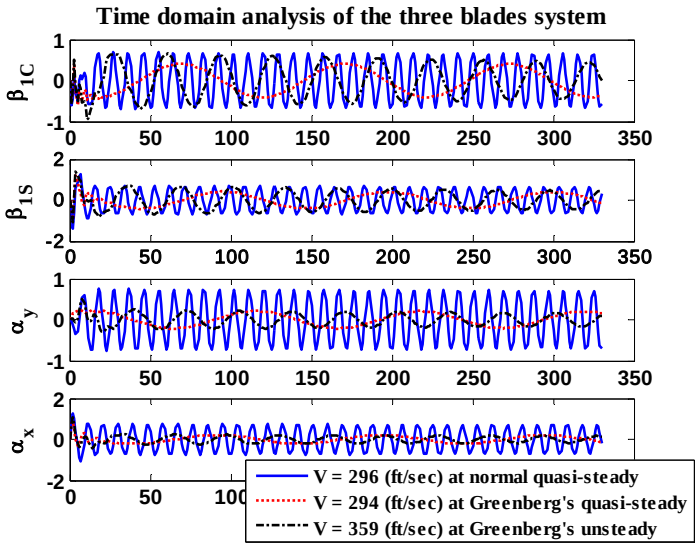

Figure 11: Time domain analysis at the respective flutter condition by each aerodynamic model

Figure 12 shows the result when varying the pylon stiffness under the full unsteady aerodynamics. The nominal flutter speed is based on the results in Fig. 10. It is very clear that the whirl flutter boundary is linearly improved by increasing the pylon stiffness until about 10% relative to its nominal value.

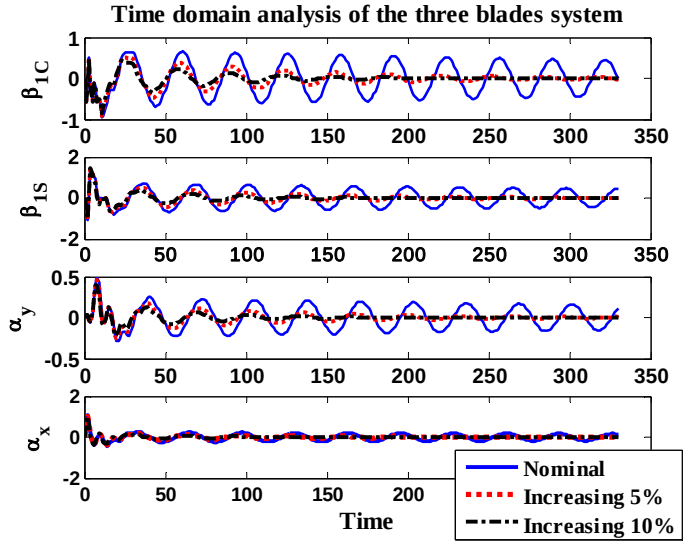

Figure 12: Results with respect pylon stiffness based on full unsteady aerodynamics

4 CONCLUSION

Time and frequency domain analyses are conducted using a newly developed assessment tool on passive control methodologies for whirl flutter stability in tiltrotor aircraft. The following conclusions can be derived from this study.

1. A new assessment tool, which enables evaluation of the passive control methodologies, is established to analyze whirl flutter stability in time and frequency domain.

2. The full unsteady aerodynamic theory predicts the whirl flutter instability to occur at a higher flight velocity than quasi-steady aerodynamic models do.

3. Passive control algorithms, which are to vary the pylon stiffness and the pitch-flap coupling, are examined to improve the whirl flutter stability boundary. From the analysis results, it is found that each system has an optimum pitch-flap coupling value. Also, its stability boundary is linearly increased in proportion to the pylon stiffness. The stability results by the quasi-steady aerodynamics are found to be more conservative than those obtained by the full unsteady aerodynamic model.

5 ACKNOWLEDGEMENTS

This work was supported partially by grant No. R01-2005-000-10059-0 from the Basic Research Program of the Korea Science & Engineering Foundation, the Korea Research Foundation, and the Korean Federation of Science and Technology Societies Grant funded by the Korean Government (MOEHRD, Basic Research Promotion Fund).

6 REFERENCES

[1] Hall, Jr., W. E., "Prop-Rotor Stability at High Advance Ratios," *Journal of the American Helicopter Society*, Vol. 11, No. 2, April 1966, pp.11-26.

[2] Kvaternik, R. G. and Kohn, J. S., "An Experimental and Analytical Investigation of Proprotor Whirl Flutter," NASA Technical Paper-1047, Dec, 1977.

[3] Johnson, W., "Optimal Control Alleviation of Tilting Prorotor Guest Response," *Journal of Aircraft*, Vol. 14, No. 3, March 1977, pp. 301-308.

[4] Nixon, M. W., Kvaternik, R. G., and Settle, T. B., "Tiltrot Vibration Reduction Through Higher Harmonic Control," American Helicopter Society 53rd Annual Forum, Virginia Beach, Virginia, April 29-May 1, 1977.

[5] Singh, R. and Gandhi, F., "Wing Flaperon and Swashplate Control for Whirl flutter Stability Augmentation of a Softinplane Tiltrotor", The 31st European Rotorcraft Forum, Florence, Italy, Sept. 13-15, 2005.

[6] Kvaternik, R. G., Piatak, D. J., Nixon, M. W., Langston, C. W., Singleton, J. D., Bennett, R. L., and Brown, R. K., "An Experimental Evaluation of Generalized Predictive Control for Tiltrotor Aeroelastic Stability Augmenttion in Airplane Mode of Flight," American Helicopter Society 57th Annual Forum, Washington, DC, May 9-11, 2001.

[7] Johnson, W., "Dynamics of Tilting Proprotor Aircraft in Cruise Flight," NASA Technical Note D-7677, May, 1974.

[8] Bisplinghoff, R. L., Ashley, H., and Halfman, R. L., *Aeroelasticity*, Dover, New York, 1996.

[9] Theodorsen, T., “General Theory of Aerodynamic Instability and the Mechanism of Flutter,” National Advisory Committee for Aeronautics - Reports, No. 496, 1935.
[10] Dinyavari, M. A. H. and Friedmann, P. P., “Application of Time-Domain Unsteady Aerodynamics to Rotary-Wing Aeroelasticity,” *AIAA Journal*, Vol. 24, No. 9, 1986, pp. 1424-1432.
[11] Jones, R. T., “The Unsteady Lift of a Wing of Finite Aspect Ratio,” NACA Report 681, 1940.
[12] Jones, R. T., “Operational Treatment of the Nonuniform Lift Theory to Airplane Dynamics,” NACA TN 667, 1938.
[13] Friedmann, P. P., and Robinson, L. H., “Influence of Unsteady Aerodynamics on Rotor Blade Aeroelastic Stability and Response,” *AIAA Journal*, Vol. 28, No. 10, December 1990, pp. 1806-1812.